Changes in Aerosols, Meteorology, and Radiation in the Southeastern U.S. Warming Hole Region during 2000 to 2019

VIRENDRA P. GHATE,[a] ANNMARIE G. CARLTON,[b] THOMAS SURLETA,[c] AND ALYSSA MARIE BURNS[b]

[a] *Argonne National Laboratory, Lemont, Illinois*
[b] *University of California, Irvine, Irvine, California*
[c] *Actalent Services, Chicago, Illinois*

(Manuscript received 1 February 2022, in final form 29 June 2022)

ABSTRACT: Surface air temperatures in the southeastern United States that did not change from the climatological mean from 1900 to 2000 have increased since the year 2000. Analyzed herein are factors modulating the surface air temperatures in the region for a 20-yr period (2000–19) using space- and surface-based observations, and output from a reanalysis model. The 20-yr period is segregated into two decades, 2000–09 and 2010–19, corresponding to different tropospheric chemical regimes. Changes in seasonal and decadal averages are examined. The later decade experienced higher average surface air temperatures with significant warming during summer and fall seasons. Decadal and seasonal averages of cloud properties, column water vapor, rain rates, and top-of-atmosphere outgoing longwave radiation did not exhibit statistically significant differences between the two decades. The region experienced strong warm and moist advection during the winter months and very weak advection during the summer months. The later decade exhibited higher low-level moisture advection during the winter months than the earlier decade with insignificant changes in the temperature advection between the two decades. The later decade had significantly lower aerosol dry and liquid water mass during all seasons, along with lower aerosol optical depth, higher single scattering albedo, and lower top-of-the-atmosphere outgoing shortwave radiation during cloud-free conditions in the summer season. Collectively, these results suggest that changes in the aerosol direct radiative forcing are responsible for warming during summer months that experience weak advection and highlight seasonal differences in the temperature controlling mechanisms in the region.

KEYWORDS: Aerosols; Shortwave radiation; Aerosols/particulates

1. Introduction and motivation

Although surface air temperatures over much of the world have warmed by ~0.5 K between 1901 and 2000 (Hartmann et al. 2013), the surface air temperatures in the southeastern United States (SEUS) did not exhibit any warming (Fig. 1a) during that period (Kunkel et al. 2006; Meehl et al. 2012; Pan et al. 2004; Portmann et al. 2009; Fall et al. 2021). This lack of warming has been termed as the "warming hole" and has been affirmed by long-term ground-based and satellite observations. However, the strength and spatial extent of the warming hole have decreased over the last two decades (Fig. 1b). Although the spatial extent of the warming hole has decreased post-2000, the temperatures within the SEUS are still colder than their climatological values as compared to those in the rest of the United States (Fig. 1c). The processes responsible for causing and modulating the strength and extent of this warming hole have been much studied (e.g., Carlton et al. 2018) and debated with studies proposing it to be a result of any or all of the following: "dimming" due to aerosols (Leibensperger et al. 2012; Mickley et al. 2012; Saxena and Yu 1998; Tosca et al. 2017; Silvern et al. 2017; Zheng et al. 2020); an increase in cloudiness, precipitation, and soil moisture variability (Napton et al. 2010; Liang et al. 2006; Yu et al. 2014; Cusworth et al. 2017); variability of sea surface temperatures (SSTs) in both the Atlantic and Pacific (Kunkel et al. 2006; Wang et al. 2009); reduced sensible heat loss due to increased irrigation (Puma and Cook 2010; Misra et al. 2012); and changes in land use/land cover (Ellenburg et al. 2016).

Meehl et al. (2012) showed that the strength and extent of the warming hole were largest in the winter season and that the hole is caused by a large-scale atmospheric circulation anomaly pattern that advected colder air to the region. In a subsequent study, Meehl et al. (2015) traced these anomalous circulation patterns to be due to a positive phase in the interdecadal Pacific oscillation (IPO). They also showed that the IPO transitioned to a negative phase in the late 1990s and thereby the region came under a wintertime southerly warm air advection, and they predicted the disappearance of the warming hole after about 2000. Although substantial warming has occurred since 2000 primarily in the winter season, the warming hole is still present in the long-term temperature anomaly trend with a reduced spatial extent and magnitude, with the warming during spring, summer, and fall being much weaker as compared to the wintertime warming.

It remains unclear to what extent the recent warming was controlled by the wintertime temperature advection versus increased greenhouse gas (GHG) concentrations. It is further

Denotes content that is immediately available upon publication as open access.

Supplemental information related to this paper is available at the Journals Online website: https://doi.org/10.1175/JCLI-D-22-0073.s1

Corresponding author: Virendra P. Ghate, vghate@anl.gov

DOI: 10.1175/JCLI-D-22-0073.1

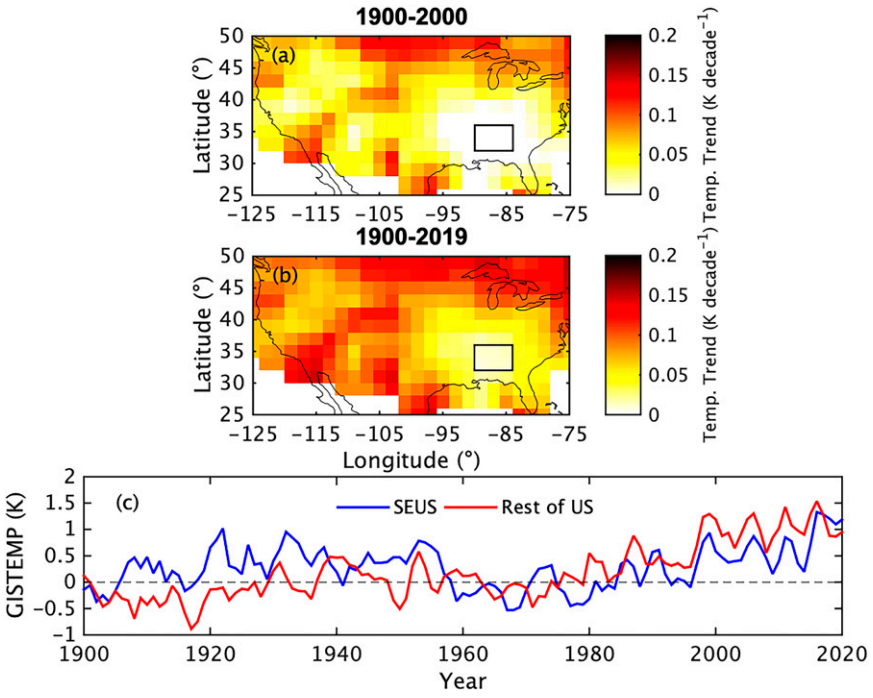

FIG. 1. Long-term trend of annual averaged surface air temperature anomaly (GISTEMP) within the continental United States for (a) 1900–2000 and (b) 1900–2019. (c) Annual mean surface air temperature anomaly in the SEUS (black rectangle) and the rest of the United States.

unclear how changes in factors (other than GHG) that govern regional radiation budgets (e.g., cloud, aerosol, land surface properties) and their seasonality affect the annual and seasonal temperature trends. To address these issues, we analyzed 20 years (2000–19) of meteorological, cloud, aerosol, chemical, and optical data collected by variety of satellite remote sensing instruments, reanalysis models, and surface aerosol measurements. Consistent with Meehl et al. (2015), the trend in the wintertime surface air temperatures in the SEUS was positive during 2000–19; however, the warming was more pronounced during the later decade (2010–19) than the earlier decade (2000–09) (Fig. 2). The spring and summer seasons did not exhibit any trend in the surface air temperature anomalies, whereas much of the warming occurred in the fall season during 2010–19 as compared to that during 2000–09. Although the seasonal and annual average trends in surface air temperature anomalies on decadal time scales are good indicators of the warming due to increased GHG concentrations, it is difficult to trace their relation to the other factors that modulate the regional radiation budget (aerosol, clouds, water vapor, etc.). It is not possible to calculate the "change from the climatic mean" of these radiation modulating variables as it is done to calculate surface air temperature anomaly values (GISTEMP) due to lack of reliable measurements of these variables prior to 2000. In addition, meteorological, clouds, and aerosol fields exhibit a distinct seasonal cycle yielding a large spread in annual average values, and the 20 years of data is insufficient to probe statistically significant changes in the trends in these properties. Hence, rather than investigating trends in these properties, we utilize the 20 years of data (2000–19) to examine the changes in their values during the two decades, 2000–09 and 2010–19. The chemical regime of the southeastern U.S. atmosphere changed in response to the 1990 Clean Air Act Amendments and other factors, such as improved energy efficiency and economic recession (Carlton et al. 2018). Implementation of the Clean Air Interstate Rule (CAIR) began reducing emissions of NO_x in 2009 and SO_2 in 2010. These species contribute to formation of hygroscopic sulfate and nitrate particle mass, and this is a motivating factor for the decade choice. Furthermore, it is problematic to probe the seasonal or annual trends in the radiation modulating variables during the two decades due to limited sample size (10), as a single outlying value can severely affect the trend (slope) calculation. This is visible in the trends in the summer and spring season temperatures during 2010–19 (Fig. 2), as 2010 had an unusually warm summer and 2012 had an unusually warm spring, yielding cooling trends during these seasons. As shown later, the 2010–19 summers were on average warmer than the 2000–09 summers, and temperatures did not exhibit statistically significant changes during the spring season. The strong positive trend in the surface air temperature during the 2010–19 winter season is partly driven by an unusually colder winter in 2010. As shown later, on average the surface air temperatures were not different between the two decades. Figures showing the seasonally averaged surface air temperature anomalies in the SEUS for the two decades, as well as seasonal trends during 2000–19, are in the online supplemental material. This issue is further discussed in the last section.

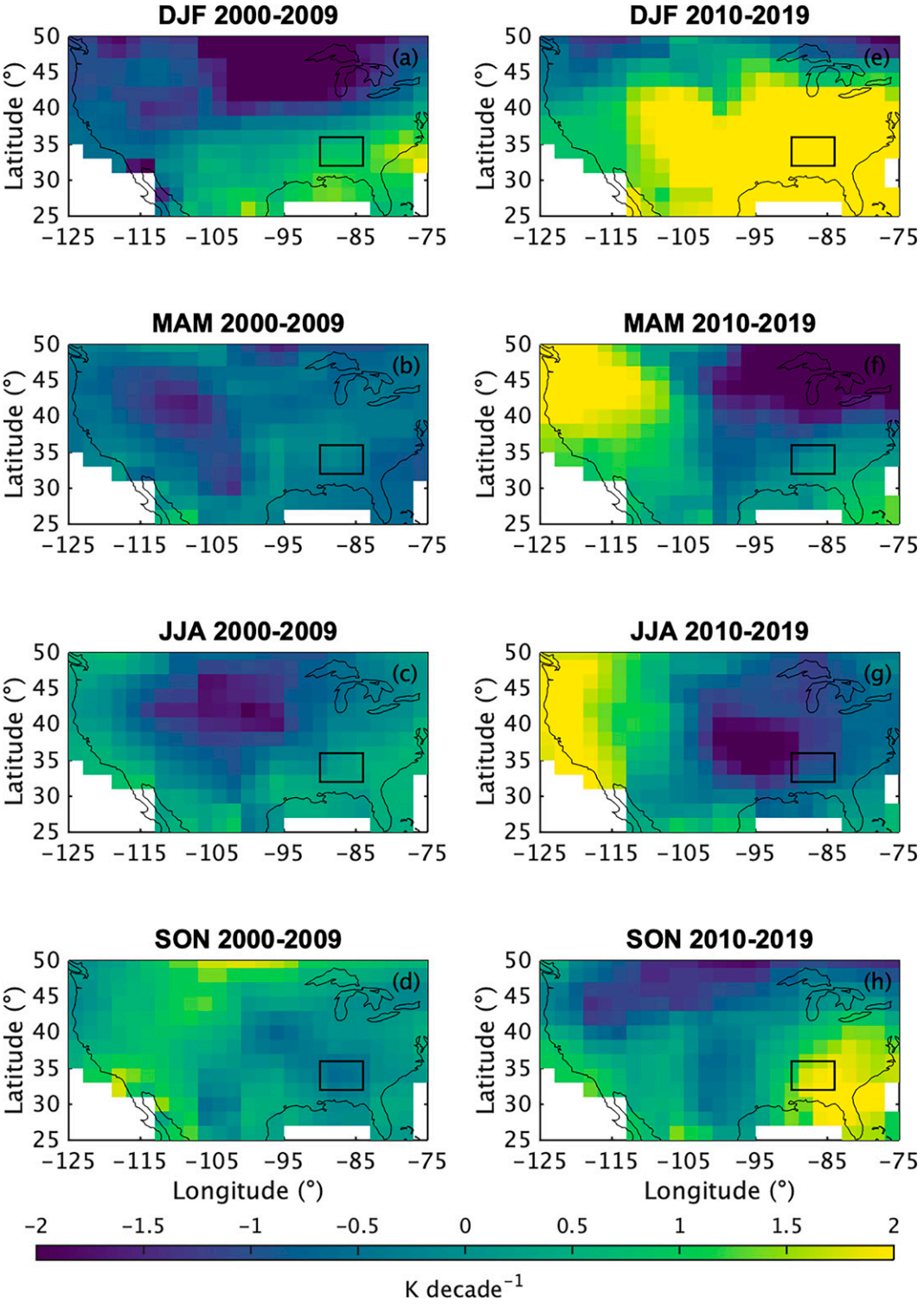

FIG. 2. Trend in seasonally averaged surface air temperature anomaly (GISTEMP) during (a)–(d) 2000–09 and (e)–(h) 2010–19. The study region is shown in the black rectangle.

TABLE 1. Sources and characteristics of dataset used in this work. Please refer to the text for references on data and uncertainty.

Source platform	Variables used	Characteristics
Goddard Institute of Space Studies (GISS) surface temperature analysis (GISTEMP)	Surface air temperature anomalies from 2000 to 2019	2° spatial and monthly temporal; uncertainty of 0.17 K
Interagency Monitoring of Protected Visual Environments (IMPROVE)	Calcium, magnesium, nitrate, potassium, sodium, sulfate, and total fine mass concentrations	Monthly averaged from two surface sites (COHU1 and SIPS1); uncertainties are reported as measure of standard deviation and are generally low (<10%) for most species
Moderate Resolution Imaging Spectroradiometer (MODIS)	Aerosol optical depth (AOD), single scattering albedo (SSA), angstrom exponent (AE), integrated water vapor (IWV), liquid water path (LWP), cloud fraction, and land albedo	1° spatial and monthly temporal for aerosol and cloud properties; 500 m and daily for land surface albedo; uncertainty in AOD of 0.03 + 20%, IWV of 13%, LWP between 4 and 40 g m^{-2}, and albedo of 5%
Integrated Multi-satellitE Retrievals for GPM (IMERG)	Rain rate	Monthly averaged at 0.1° spatial resolution; average uncertainty in the region of 0.36 mm day^{-1}
Clouds and the Earth's Radiant Energy System (CERES) Energy Balanced and Filled (EBAF) fluxes	Top-of-atmosphere (TOA) longwave (LW) and shortwave (SW) fluxes during clear-sky and all-sky conditions	Monthly averaged at 1° spatial resolution; uncertainty of 5 W m^{-2} in both longwave and shortwave fluxes
European Centre for Medium-Range Weather Forecasts reanalysis model (ERA5)	Profiles of temperature, water vapor mixing ratio, and boundary layer height	—

The data and methods are described in section 2, followed by section 3, which describes the comparisons of seasonal and annual changes in meteorological, aerosol, and land surface properties. The article is concluded with a summary and discussion in section 4.

2. Data

Data from various sources collected between January 2000 through December 2019 within the study area that is bounded by the northwest corner at 36°N, 90°W and southeast corner at 32°N, 84°W were utilized (Table 1). The Goddard Institute of Space Studies (GISS) surface temperature analysis version 4 (GISTEMP) data are used in this study (Lenssen et al. 2019). The data contained monthly values of surface air temperature anomalies from the climatic mean.

Chemical composition of ambient fine particulate matter (PM2.5) at the surface as reported by the Interagency Monitoring of Protected Visual Environments (IMPROVE) sites were used in this work (http://vista.cira.colostate.edu/Improve/). Although four IMPROVE sites are present in the study area, only two of them were operational over the entire two decades: SIPS1 (34.34°N, 87.33°W), and COHU1 (34.78°N, 84.62°W). The IMPROVE sites collected PM2.5 samples to chemically characterize organic carbon (OC), elemental carbon (EC), sulfate, nitrate, and other ions (Hyslop and White 2008). Aerosol liquid water (ALW) is lost from PM2.5 filter samples, and hence we estimated ALW mass concentrations to reconcile filter-based measurements with satellite-derived AOD estimates (Nguyen et al. 2016; Babila et al. 2020). We assumed metastable particles and calculated ALW mass with a publicly available thermodynamic equilibrium model, ISORROPIA (Fountoukis and Nenes 2007). The ALW estimates were further integrated from surface to the depth of the planetary boundary layer to calculate the aerosol water path (AWP). The ERA5 reported thermodynamic variables (described next) were used in these calculations.

Due to a lack of collocated thermodynamic and chemical observations within the region, the surface (2 m) and profiles of temperature, and water vapor mixing ratio, along with the estimates of depth of the planetary boundary layer (PBL) as estimated by the European Centre for Medium-Range Weather Forecasts (ECMWF) reanalysis model (ERA5) were used in this work (Hersbach et al. 2020). The fields available at a 0.25° spatial resolution and hourly time scales were paired in space and time with the IMPROVE sites. Daily averaged data at locations of the two sites were first averaged on monthly time scales, and then averaged together to produce a monthly value for the entire region. The monthly averaged profiles of water vapor and temperature advection were calculated using the region-mean winds and the difference between 1°-wide averages in the north–south and east–west directions.

Monthly averaged cloud and aerosol properties as observed by the Moderate Resolution Imaging Spectroradiometer (MODIS) onboard the *Terra* satellite were used in this work (Platnick et al. 2017; King et al. 2013). We have utilized the aerosol properties as derived from the Deep Blue algorithm (Sayer et al. 2013) as we mainly focus on aerosols that influence the visible spectral region, rather than other aerosols that influence the near-infrared or infrared region (e.g., dust). Hence, the aerosol optical depth (AOD) and the single scattering albedo (SSA) at 470 nm wavelength along with the calculated angstrom exponent (412–470 nm) are analyzed in this work. The integrated water vapor (IWV) values as derived

using the near-infrared algorithm are used, and hence correspond to the daytime values during cloud-free periods (Gao et al. 2015). The cloud liquid water path (LWP) as derived by the visible/near-infrared algorithm, as derived through its relationship with cloud optical thickness and drop effective radius are used (Zhou et al. 2016). The MODIS *Terra* data were available at a uniform 1° spatial resolution on monthly time scales beginning from February 2000 and were then averaged within the study area.

The monthly averaged rain rates as reported by the Global Precipitation Measurement (GPM)'s Integrated Multi-satellitE Retrievals for GPM (IMERG) data are used in this work. The GPM data are available at a 0.1° spatial resolution on monthly time scales (Huffman et al. 2018, 2020). The top of the atmosphere (TOA) shortwave and longwave fluxes during cloudy and clear-sky (cloud-free) periods as reported by the Clouds and the Earth's Radiant Energy System (CERES) project are utilized. The CERES Energy Balanced and Filled (EBAF) fluxes utilize the MODIS observed cloud properties and other variables as reported by Loeb et al. (2018) and Kato et al. (2018) and are available at 1° spatial and monthly temporal resolution.

The MODIS bidirectional reflectance distribution function (BRDF)/albedo parameters available at 500 m spatial resolution at daily time scales were used in this study (Schaaf et al. 2002). The spectral albedos derived in seven bands were then used to calculate the albedo in the shortwave (0.4–3 μm) band. Specifically, we used the MCD43C3 climate modeling grid (CMG) albedo product (MODIS/Terra Albedo Daily L3 Global 0.05 deg CMG) that provides both the white-sky albedos and the black-sky albedos (at local solar noon). The monthly averaged values of the band-averaged albedos are used in this work.

As most of the meteorological, cloud, aerosol, and land surface properties in the region exhibit a distinct annual cycle, changes within different seasons were explored. For this analysis we defined the winter season as December–February, spring as March–May, summer as June–August, and fall as September–November. In addition, the differences in all the monthly data within the two decades ("All") are also examined to understand the seasons most impacting the annual means that are usually used in studies focused on long-term statistics.

3. Results

The global average (±1 standard deviation) carbon dioxide concentration during 2000–09 was 378 ± 6 ppm and during 2010–19 was 400 ± 7 ppm (www.esrl.noaa.gov/gmd/ccgg/trends/), and the surface air temperature anomalies in the study area were 0.41 ± 0.52 K and 0.79 ± 0.94 K, respectively. These decadal average changes in CO_2 concentration and surface air temperature in the SEUS were statistically significant at a 5% confidence interval assuming a two-tailed Gaussian distribution. Hence, the relative changes in the parameters affecting surface air temperature within the two subsets serve as a convenient way of understanding the changes in the warming hole during the last 20 years.

a. Cloud and meteorological variables

Surface air temperature can be modulated by changes in cloud properties (coverage, condensate loading, etc.) through their impact on radiation, and changes in meteorological fields (vapor loading, precipitation, advective tendencies, etc.). Hence, we first diagnosed whether such properties exhibited any changes between the two decadal periods overall and by season.

The surface air temperatures were on average warmer during the later decade as compared to the earlier decade, with statistically significant changes in the summer and fall seasons (Fig. 3). The average surface air temperature anomaly was not statistically different during the winter season between the two decades; however, the range of positive (warm) temperature anomaly was highest during winter and fall. Although the wintertime average surface air temperature anomalies during the two decades were not statistically different, the medians during the two decades were statistically different, indicating some amount of warming during the winter season. Although there was a strong warming trend shown in Fig. 2 during the winter seasons of 2010–19 as compared to that during 2000–09, the trend was insufficient to cause a statistically significant increase in the air temperatures. This is also a reflection of the larger variability of surface air temperatures in the winter months as compared to the summer months on the calculated trends (slope) and means during the respective decades. The analyzed Southeast region was warmer during 2010–19 as compared to 2000–09 with the warming predominantly occurring during the summer and fall seasons.

There was no statistically significant difference in cloud fraction, integrated water vapor, liquid water path, or rain rate across the two decades. The column integrated water vapor and the liquid water path demonstrate seasonal patterns that are out of phase relative to each other. IWV was highest in the summer months and lowest in the winter months; LWP was highest in the winter months and lowest in the summer months. The cloud fraction did not exhibit any distinct annual cycle or differed in the values during the two decades. This was mirrored by the surface rain rates. The faster rate of warming during the later part of the 20-yr period cannot be fully explained by cloud fraction, integrated water vapor, or liquid water path, which did not exhibit statistically discernible differences with time for the region.

Both the temperature and moisture advection exhibit a distinct annual cycle with higher values during the winter months and lower values during the summer months (Fig. 4). As shown by Meehl et al. (2015), there is warm air advection due to wintertime southerly winds. On average, the depth of the warm advection during the winter months increased along with a small insignificant increase in strength. There has been no detectable change in the strength of temperature advection during the summer and fall season. The southerly advection during the winter months also brought moist air below 900 hPa from the Gulf of Mexico. The strength of the moisture advection below 900 hPa exhibited a statistically significant increase during the later decade as compared to the earlier one. Although significant, this increase in moisture advection has not led to any changes in the column water vapor and cloudiness

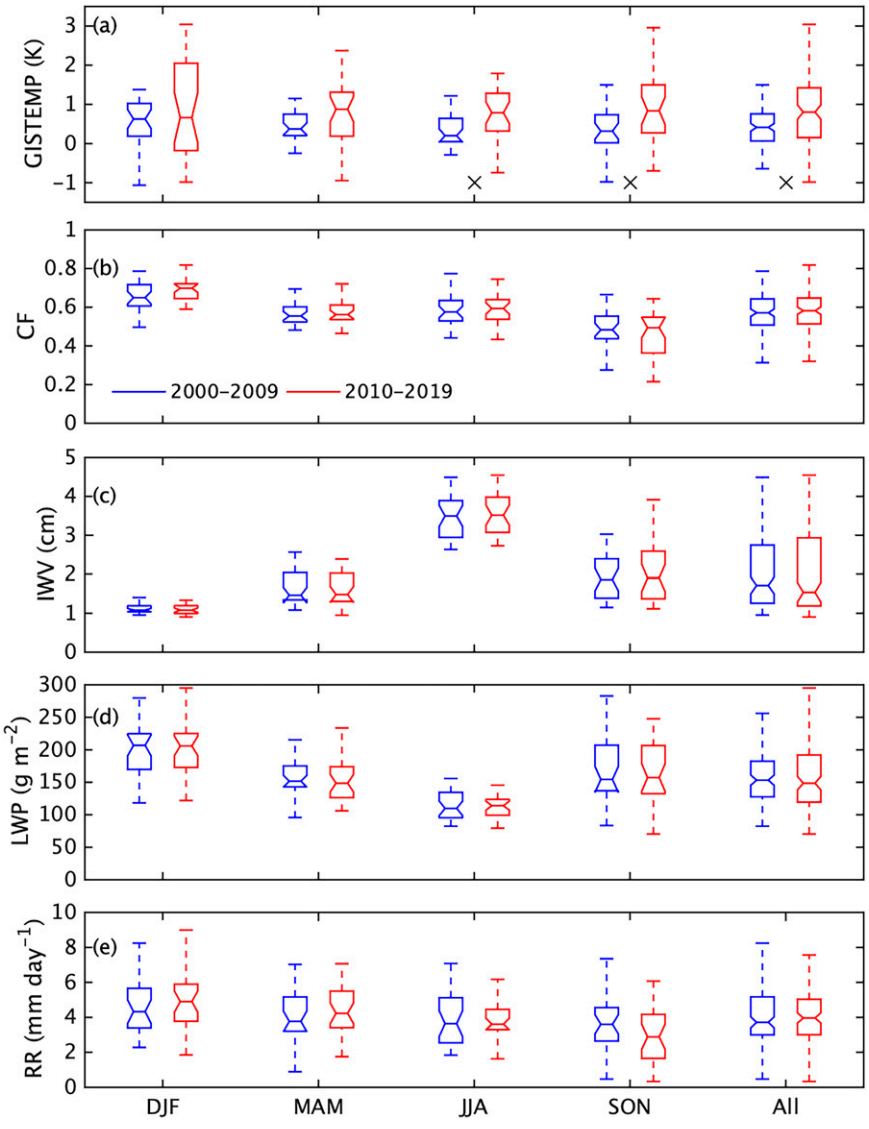

FIG. 3. Box-and-whisker plots of monthly values of (a) surface air temperature anomaly from GISTEMP, (b) cloud fraction, (c) integrated water vapor, (d) liquid water path, and (e) rain rate during 2000–09 (blue) and 2010–19 (red). The × symbol below the box and whiskers denotes if the averages of the two distributions are statistically different at a 95% confidence interval.

during the winter season (Fig. 3) in the region, thereby suggesting that the changes are insufficient to affect the local meteorology and cloud fields.

b. *Aerosol properties*

Aerosols can affect the surface air temperatures by affecting the local radiation budget through their ability to scatter and absorb solar radiation, and by altering cloud fields. There was no statistically discernible difference in cloud fields for the region over the 20 years. Hence, we examine the aerosol mass and radiative properties (Fig. 5). Due to the implementation of the Clean Air Act, there have been substantial changes in the aerosol fields between the two decades, in particular sulfate (Hand et al. 2012) a chemical species that modulates water uptake (Nguyen et al. 2016). The aerosol dry mass concentration and aerosol water path (AWP) exhibited a statistically significant decrease in all seasons during 2010–19 as compared to the values during 2000–09. Both parameters also exhibited a distinct annual cycle with the highest values during the summer months and lowest values during the winter months. The AOD, which measures the amount of radiation scattered by the aerosols at a particular wavelength, exhibited a statistically significant decrease in the decadal mean values. However, while mass and AWP decreases were significant every season, significance in AOD was observed only in the spring and summer seasons. The percent decrease in AOD was highest in the summer season,

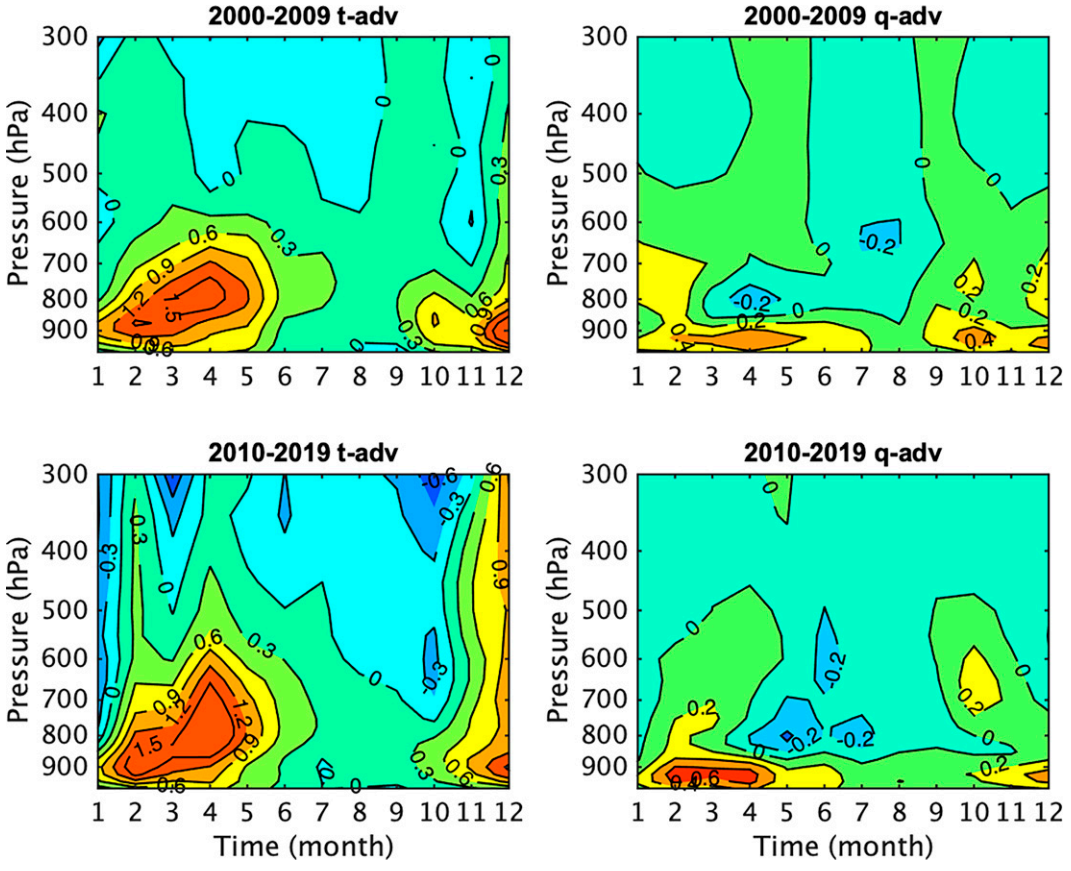

FIG. 4. Monthly average profiles of (left) temperature advection (K day^{-1}) and (right) moisture advection (g kg^{-1} day^{-1}) for (top) 2000–09 and (bottom) 2010–19.

indicating the aerosol impact on radiation budget to be highest in summer months. This surface-based observation is consistent with earlier findings that demonstrate a summertime enhancement in space-based AOD over the region (Goldstein et al. 2009; Nguyen et al. 2016).

The SSA exhibited a distinct annual cycle with the highest values during the winter months and the lowest during the summer months. Over the 20 years, SSA exhibited a statistically significant increase in the later decade during winter, spring and summer months as compared to the earlier decade. The angstrom exponent (AE) exhibited a weak annual cycle with higher values in the summer and lower values in the winter months. A very small but statistically significant decrease in the AE during the later decade was observed as compared to the earlier decade. The single scattering albedo (SSA) measures the ratio of scattering efficiency to extinction efficiency, with a value of 1 denoting a fully scattering particle and a value of zero denoting a particle completely absorbing the radiation. Mass concentrations of elemental carbon, the primary absorber of shortwave radiation, decreased in the region over the 20-yr period by approximately 50% (see Fig. S4 in the online supplemental material). Although small, an increase in the SSA suggests that the particles became more efficient in scattering the radiation during the later decade as compared to the earlier decade. *Collectively, the analyses indicate a significant decrease in aerosol dry and liquid mass concentrations resulted in a decrease in AOD mainly during the spring and summer months, and a coincident increase in the SSA.*

c. *Surface and radiative properties*

Changes in the surface radiative and turbulent fluxes can also affect the local radiation budget and hence the air temperatures. The shortwave albedos, sensible heat flux (SHF) and latent heat flux (LHF) exhibited an annual cycle with higher values in the summer months and lower values during the winter months (Fig. 6). As most of the atmospheric models assume a plane-parallel atmosphere, we focus on the black sky albedo (BSA) as it corresponds to the direct normal radiation at local noon but have shown the white sky albedo for reference. The BSA exhibited a statistically significant decrease in the later decade as compared to the earlier decade, with statistically significant decrease in winter, summer, and fall. It should be noted that the retrieval of the land surface albedo is made during cloud-free conditions and changes inaccurate assumptions of aerosol loading in the retrieval can lead to errors of ~15% (Rutan et al. 2009). Hence, it is unclear

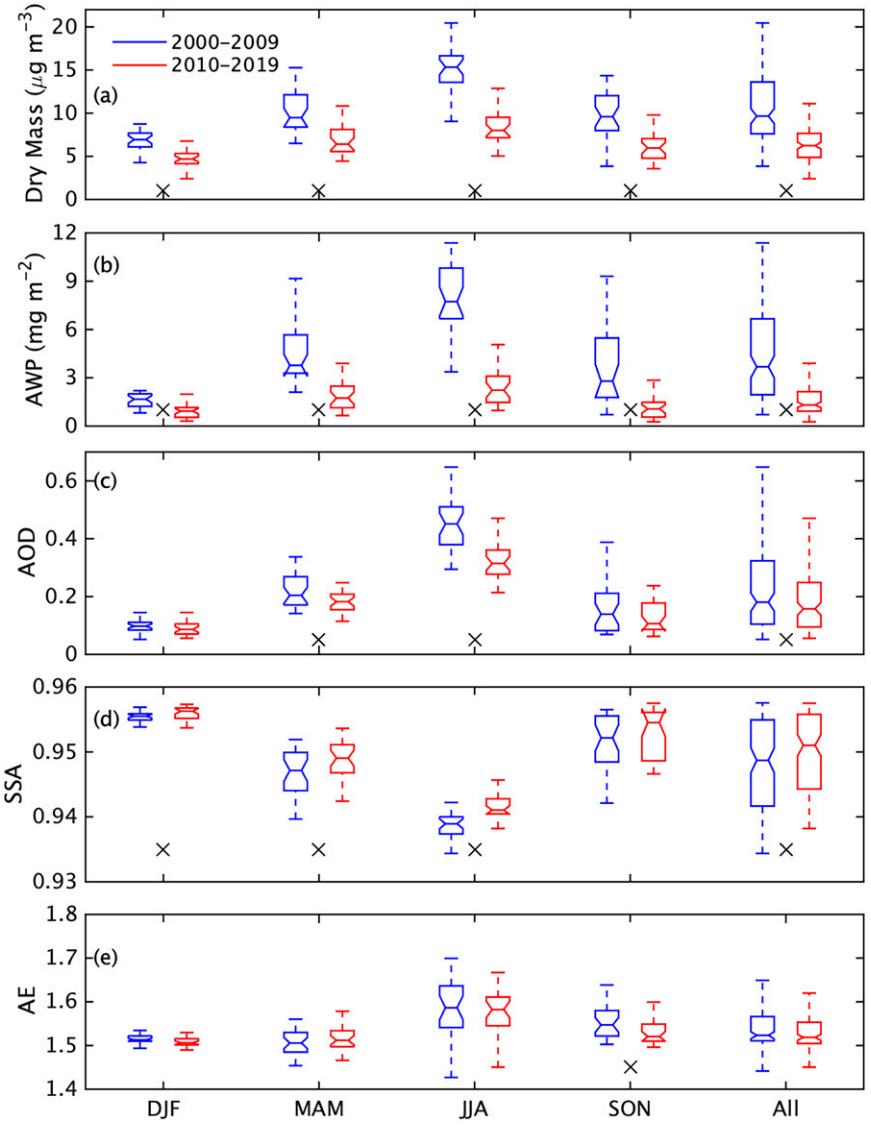

FIG. 5. Box-and-whisker plots of monthly values of (a) aerosol dry mass, (b) aerosol water path, (c) aerosol optical depth, (d) single scattering albedo, and (e) angstrom exponent during 2000–09 (blue) and 2010–19 (red). An × symbol below the box and whiskers denotes if the averages of the two distributions are statistically different at a 95% confidence interval.

whether the albedo changes observed during the summer and fall seasons are real or due to the drastic changes in the AOD during those seasons. Despite the decrease in the albedo, there is no statistically significant change in the surface SHF and LHF, suggesting that the changes are too small to affect the surface energy budget. *Overall the figure suggests a small decrease in the surface shortwave albedo in the later decade that resulted in no significant changes in the surface turbulent fluxes.*

Finally, we focus on the changes in the radiative fluxes during the two decades at the top of the atmosphere (TOA) and at the surface as these determine the surface air temperature in a one-dimensional radiation budget framework (Fig. 7). The all-sky and clear-sky (cloud-free) radiative fluxes at the surface and the TOA cloud radiative forcing did not exhibit any changes between the two decades and hence the plots are included in the online supplemental material. Both the all-sky and clear-sky TOA upwelling shortwave and longwave radiative fluxes exhibited a distinct annual cycle with higher values in the summer months and lower values in the winter months. The TOA clear-sky upwelling shortwave radiation during the summer months was lower during 2010–19 as compared to that during 2000–09. As the TOA all-sky upwelling shortwave radiation was similar for both decades, this suggests the decrease in the AOD during the later decade to be the cause of this. The TOA all-sky and clear-sky upwelling longwave

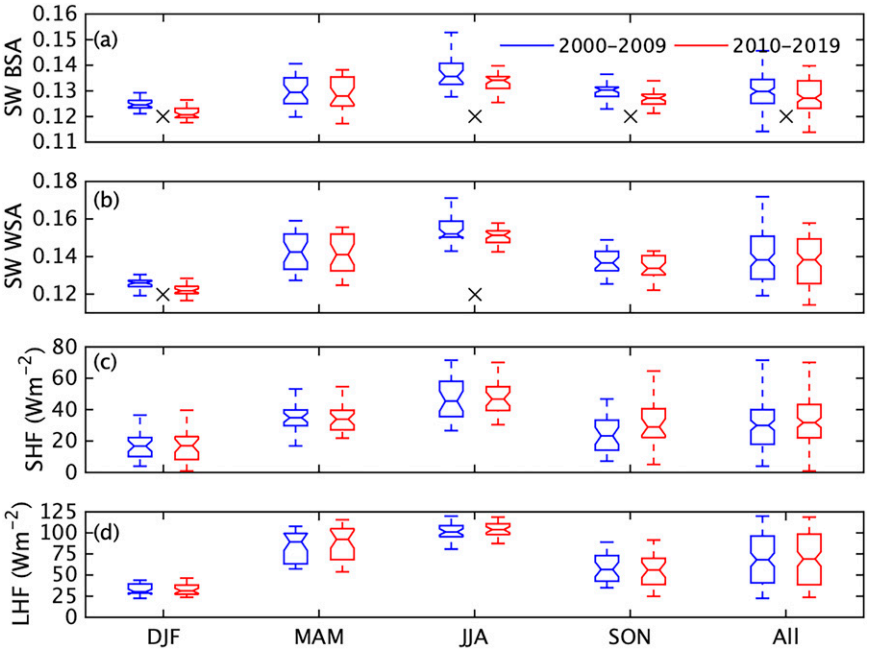

FIG. 6. Box-and-whisker plot of monthly values of (a) shortwave black sky albedo, (b) shortwave white sky albedo, (c) sensible heat flux, and (d) latent heat flux during 2000–09 (blue) and 2010–19 (red). An × symbol below the box and whiskers denotes if the averages of the two distributions are statistically different at a 95% confidence interval.

radiation did not exhibit any differences between the two decades. The lack of changes in the TOA all-sky longwave and shortwave fluxes suggest influence of clouds on the radiation budget to be unchanged during the 20-yr period. Collectively, these results suggest that the decrease in the TOA shortwave radiation during the cloud-free periods in the summer months is to a decrease in the AOD.

4. Summary, conclusions, and discussion

Unlike most of the rest of the world, the surface air temperatures have not increased significantly over the last century in the southeastern United States (SEUS), with some recent increase in the temperature leading to a decrease in the size and strength of the warming hole. This study examined the factors modulating the surface air temperature for a 20-yr period between 2000 and 2019. The 20-yr period was further divided into two 10-yr periods, 2000–09 and 2010–19. The global average surface air temperature anomaly over land was 0.76 ± 0.27 K in 2000–09 and 1.10 ± 0.3 K in 2010–19. However, in the SEUS the surface air temperature anomaly was 0.41 ± 0.52 K and 0.79 ± 0.94 K during 2000–09 and 2010–19 respectively. The results suggest that the SEUS is still colder than the rest of the world with significant warming during the last 20 years. The primary findings of our analysis based on the comparisons of the seasonal and yearly averaged properties during 2000–09 and 2010–19 include the following:

1) Statistically significant increase in surface air temperature anomaly from climatological mean with increases primarily in the summer and fall season.
2) No changes in the column water vapor, liquid water path, cloud fraction, and rain rate during 2000–19.
3) Very small statistically insignificant increase in the low-level temperature advection during the winter months, and a statistically significant increase in the low-level moisture advection during the winter months.
4) Significant decrease in the aerosol dry and liquid mass across all seasons together with a statistically significant decrease in AOD during spring and summer, and a statistically significant increase in the single scattering albedo during winter, spring, and summer.
5) A small but statistically significant decrease in the surface black-sky albedo during winter, summer, and fall, and no changes in the surface turbulent fluxes.
6) A statistically significant decrease in the TOA upwelling shortwave radiation during cloud-free periods in the summer months, and no changes in the TOA upwelling shortwave radiation during all-sky conditions, and TOA upwelling longwave radiation during both cloud-free and all-sky conditions.

Broadly the analysis agrees with the previous findings of Meehl et al. (2015) regarding low-level warm air advection during the winter months affecting the surface air temperatures in the region. However, the increases in the surface air temperatures during the winter season were not statistically significant. The statistically significant warming during the summer months, together with the significant decrease in the AOD and a significant decrease in the outgoing TOA shortwave radiation during cloud-free periods, suggest aerosols to be the primary modulators to the surface air temperatures in

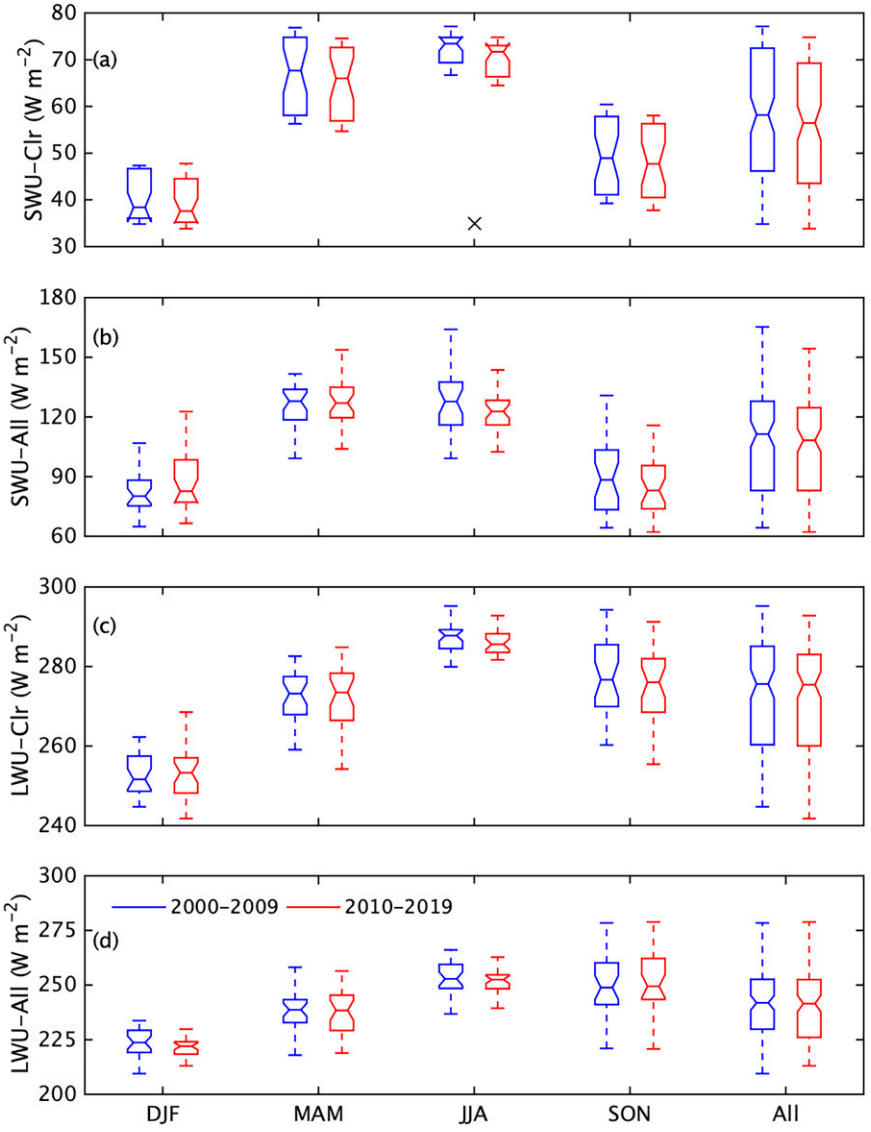

FIG. 7. Box-and-whisker plot of monthly values of top of the atmosphere (a) upwelling shortwave radiation during clear-sky conditions, (b) upwelling shortwave radiation during all-sky conditions, (c) upwelling longwave radiation during clear-sky conditions, and (d) upwelling longwave radiation during all-sky conditions during 2000–09 (blue) and 2010–19 (red). An × symbol below the box and whiskers denote if the averages of the two distributions are statistically different at a 95% confidence interval.

the region, at least during the summer months. This is further affirmed by the lack of changes in the TOA upwelling shortwave radiation during all-sky conditions and any changes in the outgoing longwave radiation as those are modulated by cloud properties. Powell and Keim (2015) analyzed surface air temperatures from 1948 to 2012 and reported a shortening of the diurnal temperature range in the SEUS region mainly due to an increase in the extreme minimum temperatures and a decrease in the extreme maximum temperatures. During the summer months the minimum temperatures are more likely to occur at night, and maximum temperatures are likely to occur during the daytime. The AOD decreased substantially from 2000–09 to 2010–19, thereby suggesting an increase in the downwelling shortwave radiation at the surface in the later decade. Hence it is plausible for the daytime high temperatures to respond and increase again as the AOD and aerosol mass continues to decrease in the future.

The contribution of the winter and fall temperatures to the variance (and range) of the annual temperatures is much higher compared to the contribution of temperatures in the spring and summer season. This, together with the low values of AOD during the earlier decade (2000–09), suggests that the annual temperatures are being modulated by the wintertime advection and not by the aerosol properties in the later

decade. Although on average the fall season during 2010–19 was warmer than that during 2000–09, none of the radiation modulating variables examined in this work exhibited a statistically significant difference between the two decades. This could be due to multiple mechanisms acting together resulting in surface warming, or to an unusually warmer 2016 fall season impacting the produced averages. The surface air temperature anomaly during 2016 fall season was 2.77 K, compared to that of 1.5 K in 2015 and 0.8 K in 2017. This further highlights the challenge associated with calculating trends (Fig. 2) or comparing averages (Fig. 3) using limited amount of data as only few samples can skew the calculated statistics.

The coincident decrease in the AOD, decrease in the TOA outgoing shortwave radiation during cloud-free conditions, and increase in the surface air temperatures during the summer months highlight the ability of aerosols to modulate surface air temperatures. This points toward formation of other warming holes in regions downwind of locations with high aerosol emissions. As the temperature and moisture advection in the SEUS during summer months is fairly weak, these "new" warming holes will perhaps also form in regions with weak advection.

Although the SEUS has increasingly experienced warm advection after 2000, the southerly winds have also brought moist air from the Gulf of Mexico. This increase in the boundary layer moisture advection in the winter months might alter the cloud field in the region in a way that might mitigate the warming. Although this analysis does not show any changes in the cloud fields or the TOA longwave fluxes in the later decade, novel surface cloud property observations made in the region such as by Atmospheric Radiation Measurement (ARM) observatories might be able to identify such changes (https://www.arm.gov/capabilities/observatories/amf/locations/seus).

Finally, the analysis shows a substantial change in the aerosol properties in the region during the last 20 years. Although the AOD has decreased substantially, the increase in the SSA is baffling. This change might be due to the decrease in the aerosol liquid water as water coated aerosol particles have lower scattering as compared to dry aerosols. This will be the focus on our further research using the detailed aerosol size and radiative properties measured at the ARM Southern Great Plains (SGP) site.

Acknowledgments. Author Ghate was supported by the U.S. Department of Energy's (DOE) Atmospheric System Research (ASR), an Office of Science, Office of Biological and Environmental Research (BER) program and the NASA's Atmospheric Composition Modeling and Analysis Program (ACMAP) under Contract DE-AC02-06CH11357 awarded to Argonne National Laboratory. We gratefully acknowledge the computing resources provided on Bebop, a high-performance computing cluster operated by the Laboratory Computing Resource Center (LCRC) at the Argonne National Laboratory. Author Carlton acknowledges support from NASA and NSF funds awarded to University of California at Irvine through Grants 80NSSC19K0987 and AGS#2024170 respectively.

Data availability statement. The data containing surface air temperature anomalies from the climatological means are available from the GISS Surface Temperature Analysis version 4 (GISTEMP v4) at https://data.giss.nasa.gov/gistemp/. The surface aerosol chemical composition data from the IMPROVE network are available at http://vista.cira.colostate.edu/Improve/improve-data/. The data from MODIS onboard the Aqua satellite are available from https://search.earthdata.nasa.gov/search by searching for "MYD08_M3.A" files. The land albedo retrieved from MODIS data are available from https://modis.gsfc.nasa.gov/data/dataprod/mod43.php/. The GPM data are freely available at https://gpm.nasa.gov/data/directory. The ERA5 data are available at https://cds.climate.copernicus.eu/. The CERES data are freely available at https://ceres.larc.nasa.gov/data/.

REFERENCES

Babila, J. E., A. G. Carlton, C. J. Hennigan, and V. P. Ghate, 2020: On aerosol liquid water and sulfate associations: The potential for fine particulate matter biases. *Atmosphere*, **11**, 194, https://doi.org/10.3390/atmos11020194.

Carlton, A. G., and Coauthors, 2018: Synthesis of the Southeast Atmosphere Studies: Investigating fundamental atmospheric chemistry questions. *Bull. Amer. Meteor. Soc.*, **99**, 547–567, https://doi.org/10.1175/BAMS-D-16-0048.1.

Cusworth, D. H., L. J. Mickley, E. M. Leibensperger, and M. J. Iacono, 2017: Aerosol trends as a potential driver of regional climate in the central United States: Evidence from observations. *Atmos. Chem. Phys.*, **17**, 13 559–13 572, https://doi.org/10.5194/acp-17-13559-2017.

Ellenburg, W. L., R. T. McNider, J. F. Cruise, and J. R. Christy, 2016: Towards an understanding of the twentieth-century cooling trend in the southeastern United States: Biogeophysical impacts of land-use change. *Earth Interact.*, **20**, 1–31, https://doi.org/10.1175/EI-D-15-0038.1.

Fall, S., K. M. Coulibaly, J. E. Quansah, G. El Afandi, and R. Ankumah, 2021: Observed daily temperature variability and extremes over southeastern USA (1978–2017). *Climate*, **9**, 110, https://doi.org/10.3390/cli9070110.

Fountoukis, C., and A. Nenes, 2007: ISORROPIA II: A computationally efficient thermodynamic equilibrium model for K^+-Ca^{2+}-Mg^{2+}-NH_4^+-Na^+-SO_4^{2-}-NO^{3-}-Cl^--H_2O aerosols. *Atmos. Chem. Phys.*, **7**, 4639–4659, https://doi.org/10.5194/acp-7-4639-2007.

Gao, B., and Coauthors, 2015: MODIS/Terra Total Precipitable Water Vapor 5-Min L2 Swath 1km and 5km. NASA MODIS Adaptive Processing System, Goddard Space Flight Center, accessed 3 December 2019, https://doi.org/10.5067/MODIS/MOD05_L2.006.

Goldstein, A. H., C. D. Koven, C. L. Heald, and I. Y. Fung, 2009: Biogenic carbon and anthropogenic pollutants combine to form a cooling haze over the southeastern United States. *Proc. Natl. Acad. Sci. USA*, **106**, 8835–8840, https://doi.org/10.1073/pnas.0904128106.

Hand, J. L., B. A. Schichtel, W. C. Malm, and M. L. Pitchford, 2012: Particulate sulfate ion concentration and SO_2 emission trends in the United States from the early 1990s through 2010. *Atmos. Chem. Phys.*, **12**, 10 353–10 365, https://doi.org/10.5194/acp-12-10353-2012.

Hartmann, D. L., and Coauthors, 2013: Observations: Atmosphere and surface. *Climate Change, 2013: The Physical Science Basis*, T. F. Stocker et al., Eds., Cambridge University Press, 159–254.

Hersbach, H., and Coauthors, 2020: The ERA5 global reanalysis. *Quart. J. Roy. Meteor. Soc.*, **146**, 1999–2049, https://doi.org/10.1002/qj.3803.

Huffman, G. J., and Coauthors, 2018: NASA Global Precipitation Measurement (GPM) Integrated Multi-satellitE Retrievals for GPM (IMERG): Algorithm Theoretical Basis Document version 5.2, 35 pp., https://gpm.nasa.gov/sites/default/files/document_files/IMERG_ATBD_V5.2.pdf.

——, and Coauthors, 2020: Integrated Multi-satellitE retrievals for the global precipitation measurement (GPM) mission (IMERG). *Satellite Precipitation Measurement*, V. Levizzani et al., Eds., Springer, 343–353.

Hyslop, N. P., and W. H. White, 2008: An evaluation of Interagency Monitoring of Protected Visual Environments (IMPROVE) collocated precision and uncertainty estimates. *Atmos. Environ.*, **42**, 2691–2705, https://doi.org/10.1016/j.atmosenv.2007.06.053.

Kato, S., and Coauthors, 2018: Surface irradiances of edition 4.0 Clouds and the Earth's Radiant Energy System (CERES) Energy Balanced and Filled (EBAF) data product. *J. Climate*, **31**, 4501–4527, https://doi.org/10.1175/JCLI-D-17-0523.1.

King, M. D., S. Platnick, W. P. Menzel, S. A. Ackerman, and P. A. Hubanks, 2013: Spatial and temporal distribution of clouds observed by MODIS onboard the Terra and Aqua satellites. *IEEE Trans. Geosci. Remote Sens.*, **51**, 3826–3852, https://doi.org/10.1109/TGRS.2012.2227333.

Kunkel, K. E., X.-Z. Liang, J. Zhu, and Y. Lin, 2006: Can CGCMs simulate the twentieth-century "warming hole" in the central United States? *J. Climate*, **19**, 4137–4153, https://doi.org/10.1175/JCLI3848.1.

Leibensperger, E. M., and Coauthors, 2012: Climatic effects of 1950–2050 changes in US anthropogenic aerosols—Part 2: Climate response. *Atmos. Chem. Phys.*, **12**, 3349–3362, https://doi.org/10.5194/acp-12-3349-2012.

Lenssen, N., G. Schmidt, J. Hansen, M. Menne, A. Persin, R. Ruedy, and D. Zyss, 2019: Improvements in the GISTEMP uncertainty model. *J. Geophys. Res. Atmos.*, **124**, 6307–6326, https://doi.org/10.1029/2018JD029522.

Liang, X.-Z., J. Pan, J. Zhu, K. E. Kunkel, J. X. L. Wang, and A. Dai, 2006: Regional climate model downscaling of the U.S. summer climate and future change. *J. Geophys. Res.*, **111**, D10108, https://doi.org/10.1029/2005JD006685.

Loeb, N. G., and Coauthors, 2018: Clouds and the Earth's Radiant Energy System (CERES) Energy Balanced and Filled (EBAF) top-of-atmosphere (TOA) edition-4.0 data product. *J. Climate*, **31**, 895–918, https://doi.org/10.1175/JCLI-D-17-0208.1.

Meehl, G. A., and Coauthors, 2012: Climate system response to external forcings and climate change projections in CCSM4. *J. Climate*, **25**, 3661–3683, https://doi.org/10.1175/JCLI-D-11-00240.1.

——, J. M. Arblaster, and C. T. Y. Chung, 2015: Disappearance of the southeast U.S. "warming hole" with the late 1990s transition of the Interdecadal Pacific Oscillation. *Geophys. Res. Lett.*, **42**, 5564–5570, https://doi.org/10.1002/2015GL064586.

Mickley, L. J., E. M. Leibensperger, D. J. Jacob, and D. Rind, 2012: Regional warming from aerosol removal over the United States: Results from a transient 2010–2050 climate simulation. *Atmos. Environ.*, **46**, 545–553, https://doi.org/10.1016/j.atmosenv.2011.07.030.

Misra, V., J.-P. Michael, R. Boyles, E. P. Chassignet, M. Griffin, and J. J. O'Brien, 2012: Reconciling the spatial distribution of the surface temperature trends in the southeastern United States. *J. Climate*, **25**, 3610–3618, https://doi.org/10.1175/JCLI-D-11-00170.1.

Napton, D. E., R. F. Auch, and R. Headley, 2010: Land changes and their driving forces in the southeastern United States. *Reg. Environ. Change*, **10**, 37–53, https://doi.org/10.1007/s10113-009-0084-x.

Nguyen, T. K. V., V. P. Ghate, and A. G. Carlton, 2016: Reconciling satellite aerosol optical thickness and surface fine particle mass through aerosol liquid water. *Geophys. Res. Lett.*, **43**, 11 903–11 912, https://doi.org/10.1002/2016GL070994.

Pan, Z., R. W. Arritt, E. S. Takle, W. J. Gutowski Jr., C. J. Anderson, and M. Segal, 2004: Altered hydrologic feedback in a warming climate introduces a "warming hole". *Geophys. Res. Lett.*, **31**, L17109, https://doi.org/10.1029/2004GL020528.

Platnick, S., M. King, and P. Hubanks, 2017: MYD08_M3 - MODIS/Aqua Aerosol Cloud Water Vapor Ozone Monthly L3 Global 1Deg CMG. NASA MODIS Adaptive Processing System, Goddard Space Flight Center, accessed 3 December 2019, https://doi.org/10.5067/MODIS/MYD08_M3.061.

Portmann, R. W., S. Solomon, and G. C. Hegerl, 2009: Spatial and seasonal patterns in climate change, temperatures, and precipitation across the United States. *Proc. Natl. Acad. Sci. USA*, **106**, 7324–7329, https://doi.org/10.1073/pnas.0808533106.

Powell, E. J., and B. D. Keim, 2015: Trends in daily temperature and precipitation extremes for the southeastern United States: 1948–2012. *J. Climate*, **28**, 1592–1612, https://doi.org/10.1175/JCLI-D-14-00410.1.

Puma, M. J., and B. I. Cook, 2010: Effects of irrigation on global climate during the 20th century. *J. Geophys. Res.*, **115**, D16120, https://doi.org/10.1029/2010JD014122.

Rutan, D., F. Rose, M. Roman, N. Manalo-Smith, C. Schaaf, and T. Charlock, 2009: Development and assessment of broadband surface albedo from Clouds and the Earth's Radiant Energy System clouds and radiation swath data product. *J. Geophys. Res.*, **114**, D08125, https://doi.org/10.1029/2008JD010669.

Saxena, V. K., and S. Yu, 1998: Searching for a regional fingerprint of aerosol radiative forcing in the southeastern US. *Geophys. Res. Lett.*, **25**, 2833–2836, https://doi.org/10.1029/98GL02106.

Sayer, A. M., N. C. Hsu, C. Bettenhausen, and M. J. Jeong, 2013: Validation and uncertainty estimates for MODIS Collection 6 "Deep Blue" aerosol data. *J. Geophys. Res. Atmos.*, **118**, 7864–7872, https://doi.org/10.1002/jgrd.50600.

Schaaf, C. B., and Coauthors, 2002: First operational BRDF, albedo and nadir reflectance products from MODIS. *Remote Sens. Environ.*, **83**, 135–148, https://doi.org/10.1016/S0034-4257(02)00091-3.

Silvern, R. F., D. J. Jacob, P. S. Kim, E. A. Marais, J. R. Turner, P. Campuzano-Jost, and J. L. Jimenez, 2017: Inconsistency of ammonium–sulfate aerosol ratios with thermodynamic models in the eastern US: A possible role of organic aerosol. *Atmos. Chem. Phys.*, **17**, 5107–5118, https://doi.org/10.5194/acp-17-5107-2017.

Tosca, M. G., J. Campbell, M. Garay, S. Lolli, F. C. Seidel, J. Marquis, and O. Kalashnikova, 2017: Attributing accelerated summertime warming in the southeast United States to recent reductions in aerosol burden: Indications from vertically-resolved observations. *Remote Sens.*, **9**, 674, https://doi.org/10.3390/rs9070674.

Wang, H., S. Schubert, M. Suarez, J. Chen, M. Hoerling, A. Kumar, and P. Pegion, 2009: Attribution of the seasonality and regionality in climate trends over the United States during 1950–2000. *J. Climate*, **22**, 2571–2590, https://doi.org/10.1175/2008JCLI2359.1.

Yu, S., and Coauthors, 2014: Attribution of the United States warming hole: Aerosol indirect effect and precipitable water vapor. *Sci. Rep.*, **4**, 6929, https://doi.org/10.1038/srep06929.

Zheng, Y., and Coauthors, 2020: Long-term observational constraints of organic aerosol dependence on inorganic species in the southeast US. *Atmos. Chem. Phys.*, **20**, 13 091–13 107, https://doi.org/10.5194/acp-20-13091-2020.

Zhou, L., Q. Liu, D. Liu, L. Xie, L. Qi, and X. Liu, 2016: Validation of MODIS liquid water path for oceanic nonraining warm clouds: Implications on the vertical profile of cloud water content. *J. Geophys. Res. Atmos.*, **121**, 4855–4876, https://doi.org/10.1002/2015JD024499.